

pubs.acs.org/NanoLett Letter

Nonequilibrium Dynamics of Electron Emission from Cold and Hot Graphene under Proton Irradiation

Yifan Yao, Alina Kononov, Arne Metzlaff, Andreas Wucher, Lukas Kalkhoff, Lars Breuer, Marika Schleberger, and André Schleife*



Cite This: Nano Lett. 2024, 24, 5174–5181



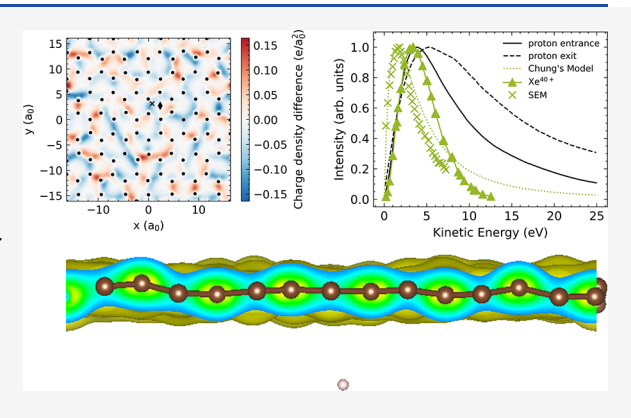
ACCESS I

III Metrics & More

Article Recommendations

sı Supporting Information

ABSTRACT: Characteristic properties of secondary electrons emitted from irradiated two-dimensional materials arise from multi-length and multi-time-scale relaxation processes that connect the initial non-equilibrium excited electron distribution with their eventual emission. To understand these processes, which are critical for using secondary electrons as high-resolution thermalization probes, we combine first-principles real-time electron dynamics with irradiation experiments. Our data for cold and hot proton-irradiated graphene show signatures of kinetic and potential emission and generally good agreement for electron yields between experiment and theory. The duration of the emission pulse is about 1.5 fs, which indicates high time resolution when used as a probe. Our newly developed method to predict kinetic energy spectra shows good agreement with electron and ion irradiation experiments and prior models. We find that the lattice temperature significantly increases secondary electron emission, whereas electron to



significantly increases secondary electron emission, whereas electron temperature has a negligible effect.

KEYWORDS: secondary electron emission, monolayer graphene, finite temperature, first-principles simulation, kinetic energy spectrum

S econdary electrons can be emitted from a target material upon the impact of ions or electrons. Their spectral and spatial distribution play a crucial role in modern light-ion microscopy to provide high-resolution surface morphology images with minimal collateral damage. ^{1–3} Emitted secondary electrons can provide important insight into the electron and ion response of the target material. ^{3–5} However, the emerging electron and ion dynamics within the target and its impact on the intensity and kinetic energy distribution of emitted secondary electrons remain elusive in experiments.

Achieving such insight requires a deep understanding of secondary electron emission as a complex multi-length and multi-time-scale process that emerges from the interaction between the incident projectile ion and the target material. It includes the dynamics of the projectile charge state, the secondary electron emission probability, and the thermalization of the radiation-induced excited electrons toward a Fermi-Dirac distribution through electron-electron scattering on the order of tens of femtoseconds. This is followed by the emergence of thermal equilibrium between nuclei and electrons through electron-phonon scattering on the order of picoseconds. These processes also involve multiple length scales: the initial interaction is localized near the impact point of the proton trajectory, while heat is subsequently transported mainly through electron diffusion with a diffusion length on the order of μ m. An analytical model of the secondary

electron kinetic energy spectra by Chung et al.⁷ is based on the work function as a barrier against emission and the electron—electron scattering mean free path governing the probability for excited electrons to diffuse to the surface. This model has successfully described the kinetic energy distribution of secondary electrons from metals under electron irradiation, and a modified version was introduced to describe secondary electrons in helium ion microscopy.⁸ These rely on the static work function of the target material as a single empirical parameter, but for a highly excited surface,⁵ the surface potential and, thus, the work function is strongly perturbed.

For bulk targets, electronic stopping has been extensively investigated, ^{9–14} and for self-irradiated silicon, first-principles simulations have shown that a highly charged ion equilibrates its charge state within a few nanometers. ¹⁵ First-principles theoretical efforts also describe the relaxation dynamics in the target. ^{16–18} Nonequilibrium dynamics is more complicated for two-dimensional (2D) systems where the impacting ion does not equilibrate its charge state before leaving the target,

Received: January 22, 2024
Revised: April 1, 2024
Accepted: April 3, 2024
Published: April 8, 2024



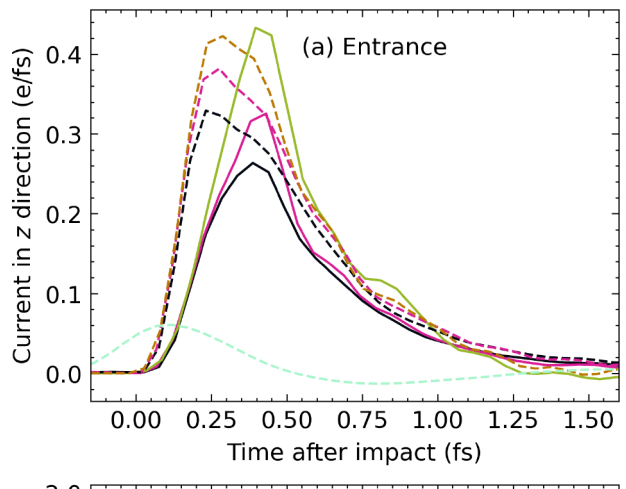


thereby leading to a response different from that of the bulk. For single- or few-layer materials, energy deposition rates, ¹⁹ charge excitation, ^{19,20} and charge capture processes ^{19,21} deviate from bulk behavior. Theoretical models for the escape probability of excited electrons for bulk⁷ rely on the electron—electron mean free path. However, this quantity is highly anisotropic in 2D systems, and the electron mean free path transverse to the graphene layer is comparable with the layer thickness.²² Besides, secondary electrons in bulk undergo scattering and can reverse their momentum, which may not occur in thin targets.²³

Experimentally, ion-surface or ion-solid interactions have been studied for decades, but direct experimental investigations of the dynamics induced by ion impact remain unfeasible. This dynamics includes thermalization within picoseconds or less through electron-electron scattering and lattice heating through electron-phonon scattering. Pumpprobe experiments can examine such subfemtosecond processes^{24,25} by interrogating the induced dynamics in the sample using lasers with attosecond pulse durations. 26-28 For ion pulses, their charge and mass constrain the reduction of monoenergetic pulse durations, and typically, only the initial state before and the final state several nanoseconds after impact are directly measurable. In addition to two-photon photoelectron emission pump-probe experiments, ²⁹⁻³¹ recent developments toward ion pump optical probe experiments³² promise sufficient temporal resolution. These allow experiments with few-picosecond ion pulses, 33-37 thereby making electronic relaxation time scales in 2D materials, such as graphene, experimentally accessible, which motivates the present work. In such modern ion beam experiments,^{33–37} the time between successive ion impacts on a sample surface reaches the few-picosecond regime. On that time scale, graphene has not yet relaxed back to its ground state and is pre-excited, that is, thermalized to a finite, nonzero temperature. Ion impact on pre-excited material can influence the secondary electron emission, but a real-time electron dynamical simulation of secondary electron emission with finite temperature is still missing.

Here, we develop a computational first-principles description of the secondary electron emission dynamics, including duration and kinetic energy spectra, for proton-irradiated graphene as a prototypical 2D material and connect with experiments. We use real-time time-dependent density functional theory (RT-TDDFT), which has successfully simulated femtosecond electron dynamics under external irradiation. ^{12,19,21,38–41} We explicitly consider the effects of nonvanishing electron and lattice temperatures of pre-excited graphene, thereby advancing understanding of secondary electrons as a probe for thermalization processes.

Our simulations show that the peak intensity of the secondary electron current in Figure 1 follows the same trend with proton kinetic energy as the secondary electron yield: ²⁰ the overall peak intensity is higher at the exit side than the entrance side with a maximum around 10 keV for the entrance and 80 keV for the exit side [see Section C in the Supporting Information (SI)]. Asymmetric ratios of exit- and entrance-side yields range from 1 to 1.5 in a comparable velocity range for hydrogen-irradiated thin carbon foils, ⁴² which is slightly below our computed ratios of 1–2.75. Higher exit-side emission has yet to be experimentally confirmed for monolayer 2D materials.



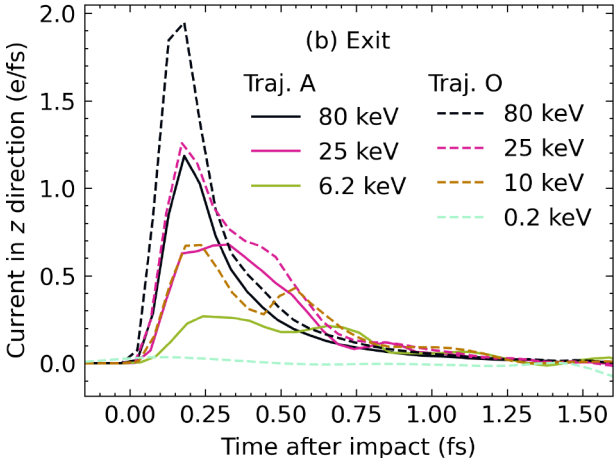


Figure 1. Simulated secondary electron current on the (a) entrance and (b) exit sides for proton-irradiated monolayer graphene (see Methods and the SI for computational details). The proton is in the graphene plane at "impact."

The difference in peak intensity (see Figure 1) and secondary electron yield (see Figure S4) near entrance and exit sides suggests that multiple emission mechanisms contribute. Potential emission of secondary electrons occurs because of potential energy released as the projectile neutralizes its charge state in the target. The magnitude of potential emission near the exit and entrance sides depends on the projectile's ionization energy and the target material's work function and Fermi velocity. 43,44 Although potential emission is more commonly discussed for highly charged ions, 5,45 the potential energy stored in the proton (13.6 eV) is almost three times the work function of graphene (4.56 eV), 46,47 which exceeds the minimum required for Auger-Meitner neutralization. 43,44 The local density approximation used in RT-TDDFT simulations (see Methods) is not expected to fully describe the Auger-Meitner process quantitatively, thereby suggesting hybrid exchange-correlation functional studies in the future. Secondary electrons due to kinetic emission are preferentially emitted at the exit side because of momentum conservation. Longer time-scale emission mechanisms involving decaying excitations within the material are expected to be symmetric with respect to the emission side.

To explore potential emission, we study a proton velocity of 0.1 at. u. (atomic units), corresponding to 0.2 keV, which is below the kinetic emission threshold estimated at 0.13 - 0.19 at. u. (0.42 - 0.9 keV). Figure 1a shows preimpact emission

for this proton kinetic energy where potential emission is expected to be the primary contribution, and the secondary electron yield for the entrance and exit sides is around 12% of the maximum yield (see Figure S4). The expression derived in ref 43, which shows fair agreement with experiment, 44,48 predicts a potential emission yield around 0.018 (see Section D in the SI), which is a value comparable with our predictions of around 0.027 (0.065) on the entrance (exit) side. The yield ratio of about 2.5 in our simulations indicates asymmetric secondary electron emission also in the potential emission regime, albeit with a small secondary electron current (Figure 1). Additionally, electron capture is most prominent for slow protons, ^{20,49} which suggests that potential emission plays a role in this regime. However, the relatively small potential energy stored in the proton leads to a small secondary electron yield compared with slow, highly charged ions.^{5,45}

We also investigate secondary electron emission experimentally (see Methods and the SI for experimental details) for two-to four-layer graphene samples since the preparation of a suitable single layer of graphene for measuring the yield is difficult. Figure 2 shows the dependence of the measured

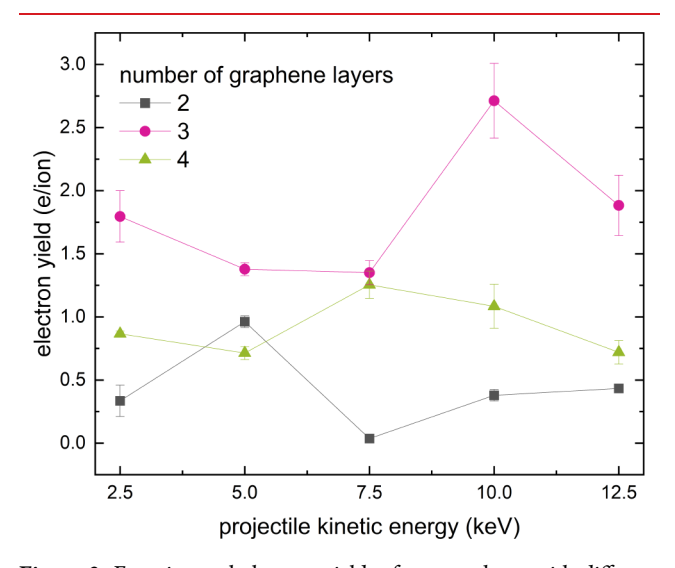


Figure 2. Experimental electron yield γ from graphene with different layer numbers as a function of projectile (Ar⁺) energy. The yield was calculated from the electron spectrum measured with the passivated implanted planar silicon (PIPS) detector by fitting a Furry distribution. Lines are a guide for the eye.

electron yield on the number of graphene layers for Ar⁺ ions with different kinetic energies. We find that there is no strong dependence on the kinetic energy of the projectile. The observed yield varies with the number of graphene layers, from 0.4, 1.8, to 0.7 electrons per ion for two-, three-, and four-layer graphene, respectively. However, this variation most likely arises from sample-to-sample variations, and we do not attribute it to a systematic thickness dependence.

The velocity of the 12.5 keV $\rm Ar^+$ ion is about 0.1 at. u., which is comparable with the velocity of the 0.2 keV proton simulation, i.e., the potential emission regime. The larger experimental yields (see Figure 2) compared with our simulations (see Figure S4) can be understood using the model of ref 43 and the ionization energy of Ar of 15.8 eV. The predicted potential emission yield (see Section D in the SI) of around 0.18 is on the same order as most of our experimental results for two-layer graphene. The factor of \sim 2

discrepancy between the experimental yields and model prediction may be attributable to the different graphene thicknesses.

Furthermore, our results in Figure 1 show that for protons with kinetic energies above the kinetic emission threshold, secondary electron emission ends after only about 1–1.5 fs. A comparable electron emission duration was reported for graphene irradiated by highly charged ions. This short time scale indicates that delayed secondary electron emission resulting from the relaxation of the energy deposited during ion impact is not observed in our simulations.

After being excited by the fast-moving proton, the emitted electrons have a range of kinetic energy depending on their initial energy state, the work function of the target, and any intermediate energy transfer processes between excitation and emission. Our simulation results in Figure 3 show a

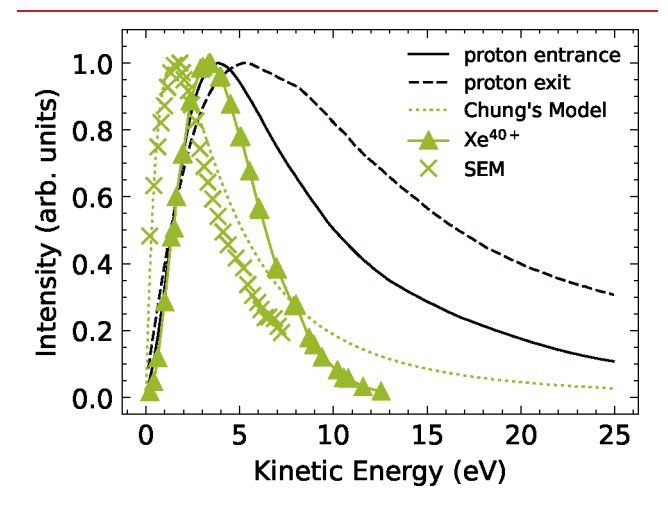


Figure 3. Comparison of our simulated kinetic energy spectra (centroid trajectory, kinetic energy of 80 keV in Figure S6) with a measured spectrum for Xe^{40+} ions impacting graphene, 45 a measured spectrum under electron irradiation in scanning electron microscopy (SEM) experiments, 51 and an analytical expression derived by Chung et al. 7 (see details in the text). The y axis is normalized to the same peak intensity.

characteristic peak around 3 eV for the entrance side and around 5 eV for the exit side. Since the peak positions do not strongly depend on impact point and proton kinetic energy (see details in Section F of the SI), we conclude that this peak is predominantly governed by intrinsic graphene material properties, such as the mean free path of excited electrons and work function. The shape of our kinetic energy spectra in Figure 3 agrees well with experimental data and the model by Chung et al., which relates the position of the secondary electron peak to 1/3 of the work function of the target. For graphene with a work function of approximately 4.56 eV, 46,47 it predicts a peak of position of 4.56/3 = 1.52 eV, which is about 2 eV below our simulation results. The scanning electron microscopy data⁵¹ is obtained in reflection geometry and comparable with our entrance side simulation data. For these data, the Chung model captures peak position and shape

In Figure 3 we also include data from highly charged Xe⁴⁰⁺ irradiation,^{5,45} which is measured in the forward direction and should be compared with our exit-side simulation data. For ion irradiation experiments, as well as our proton simulation, the kinetic energy peak appears shifted to higher kinetic energies

by about 2 eV relative to Chung's model. Although there is a modified version of this model \$^{5,51}\$ that extends it to helium irradiation, these modifications rely on fitting the energy distribution of excited electrons to experimental data. In addition, the constant value of the work function used in Chung's model will be modified by the radiation-induced electron dynamics. Other processes, such as attraction from the positively charged incident ion before impacting the target, might lead to further deviations for ion-induced emission since Chung's model is derived for electron irradiation.

Finally, we investigate pre-excited graphene, for example, due to previous ion impact. Our simulations (see Figure 1) reveal that the duration of the secondary electron pulse is only around 1.5 fs, that is, fast compared with thermalization, which indicates that the intensity of secondary electron emission can be a probe of thermalization in the target. To separate the effects of elevated electron and lattice temperatures, we investigate the proton irradiation of a cold lattice with an elevated electronic temperature and an elevated lattice temperature with cold electrons. We use electron and lattice temperatures from previous works based on two temperature models. ^{52–54}

First, we compute the secondary electron yield for an electronic temperature of 10 000 K (see Figure 4), which is

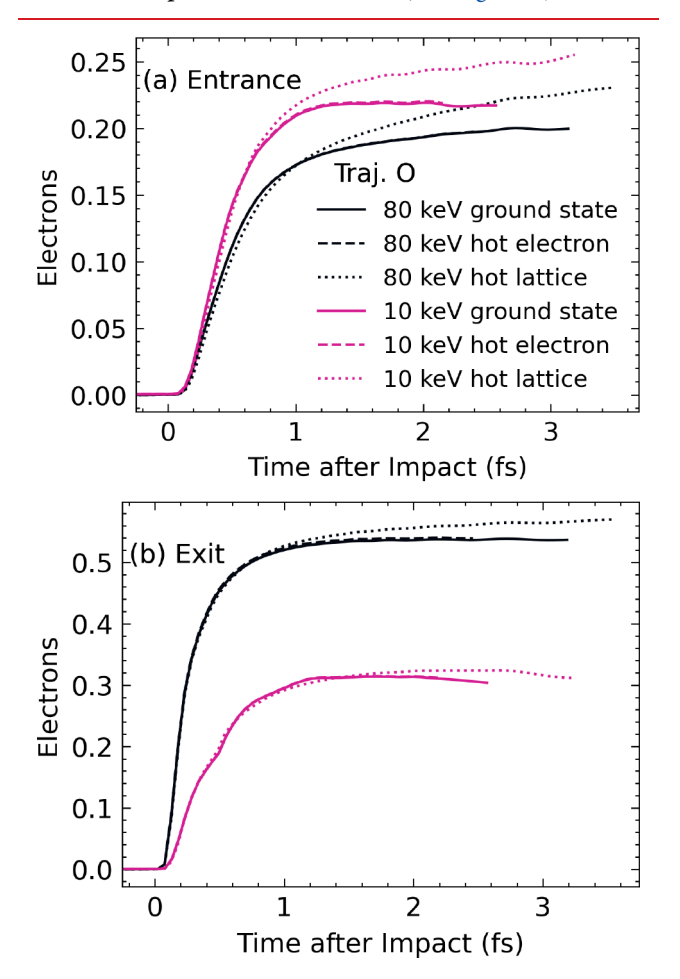


Figure 4. Number of secondary electrons computed at elevated electron temperature of $T_{\rm e}=10\,000$ K or elevated lattice temperature of $T_{\rm i}=1000$ K compared with electron emission from ground-state graphene at $T_{\rm e}=T_{\rm i}=0$ K. The proton is in the graphene plane at "impact."

achievable within the first 100 fs after the initial impact. ^{52,53} Our simulations show that the secondary electron yield is very similar to that from ground-state graphene (see Figure 4), and the effect of a high electron temperature is minor. On the contrary, Figure 4 shows that a lattice temperature of 1000 K increases the secondary electron yield by 10–13% (3–5%) on the entrance (exit) side and also for the channeling trajectory (see Figure S15). Such a lattice temperature was reported after about 400 fs from molecular dynamics simulations of ionirradiated Fe. ⁵³ Besides secondary electron yield, we simulate the kinetic energy spectrum at elevated lattice temperature (see Figure S16). The peak position and shape of the spectrum resemble those of the ground state, thereby implying that only the enhanced secondary electron yield is an indicator of lattice temperature.

To explain the modified secondary electron yield, we analyze the electron density distribution in Figure 5. We note that the

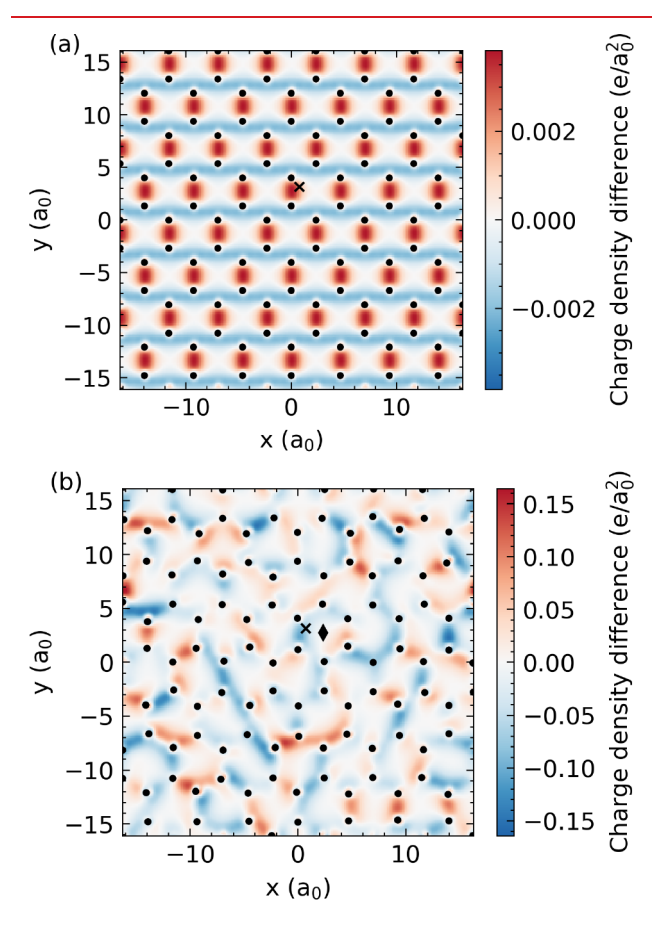


Figure 5. Comparison of the planar integrated charge density difference between elevated (a) electron ($T_{\rm e}=10\,000~{\rm K}$) or (b) lattice ($T_{\rm i}=1000~{\rm K}$) temperature and ground-state graphene for the initial state before real-time propagation. Black circles denote atomic positions of the 112 carbon atoms. The black diamond (×) denotes the proton impact point of the channeling (centroid) trajectory.

enhanced electron emission does not just depend on the charge density difference exactly at the impact point since the long-range Coulomb interaction decays as 1/r. The electron density difference at high electronic temperature is small; conversely, the difference at an elevated lattice temperature is about 2 orders of magnitude higher, which significantly modifies the interaction between projectile and target material. The electronic density of states for a hot graphene lattice

indicates a redistribution of electrons to near the Fermi energy from around -6.5 eV below it, thereby possibly facilitating their emission upon proton impact (see details in the SI).

In conclusion, we quantitatively investigate the nonequilibrium dynamics of secondary electron emission in hot and cold proton-irradiated graphene. Our simulations distinguish kinetic and potential emission in the intensity of the secondary electron yield and current for single-layer graphene. We show that the secondary electron pulse lasts about 1.5 fs, which is much faster than the subpicosecond thermalization processes of nonequilibrium electrons. The shape of the secondary electron pulse and the kinetic energy spectra agree well among the different impact parameters. Our newly derived method for calculating kinetic energy spectra agrees well with literature reports with peak positions varying by about 1-2 eV. Additionally, pre-excited graphene shows enhanced electron emission due to electron density perturbations at high lattice temperatures. Further experimental work is needed to verify predicted electron yields at nonvanishing lattice or electron temperatures. Nevertheless, we propose the characteristics of the secondary electron yield as a probe for lattice thermalization.

METHODS

We perform real-time time-dependent density functional theory simulations starting from converged ground-state single-particle Kohn—Sham (KS) states computed by using density functional theory. These are propagated in real time through the time-dependent KS equations

$$i\frac{\partial}{\partial t}\phi_{j}(\mathbf{r},t) = \left[-\frac{\nabla^{2}}{2} + V_{KS}(\mathbf{r},t)\right]\phi_{j}(\mathbf{r},t)$$
(1)

using the enforced time-reversal symmetry (ETRS) method with a time step of one attosecond. ϕ_i are single-particle KS orbitals evolving in a time-dependent effective potential V_{KS} , which is a functional of the electron density $n(\mathbf{r},t)$. Kohn– Sham states are represented using a plane-wave basis with a cutoff kinetic energy of 50 hartree. Exchange and correlation effects are treated using the adiabatic local density approximation. 57,58 The electron-ion interaction is described by norm-conserving Hamann-Schlüter-Chiang-Vanderbilt pseudopotentials. 59 The large simulation cell with 112 carbon atoms and 100 a_0 of vacuum [see Figure S2 for channeling (A) and centroid (O) proton trajectories] allows using only the Γ point for Brillouin zone sampling. All these parameters are consistent with previous work. 20,23,60 We use absorbing boundary conditions, 60 as implemented in the Qb@ll code, 61-63 to avoid unphysical re-entering of emitted electrons into a periodic image of the simulation cell (see details in the SI). We represent an elevated electronic temperature using a Fermi-Dirac distribution of KS occupation numbers within Mermin DFT.⁶⁴ An elevated lattice temperature is represented using atomic displacements from the approach in ref 65 and the SI.

Experimentally we investigate the number of electrons emitted from a free-standing graphene target under singly charged ion bombardment. The experimental setup (see Figure S1 of the SI) is based on a design developed by the Aumayr group. 66,67 The experiment operates in transmission geometry with free-standing graphene targets consisting of multiple layers (see sample preparation details in ref 32). A singly charged argon ion produced by a rare gas ion source (Atomica

Duoplasmatron) impacts the graphene target with kinetic energies of 2.5-12.5 keV, thereby leading to electron emission. Notably, no stripping effects are expected as the rather slow singly charged argon ions traverse the target, and thus, the experiments are comparable with our proton-irradiation simulations. A proton with the same velocity as an argon ion has a 40 times smaller kinetic energy. Hence, we expect that irradiation with ~ 6.2 keV protons, which is simulated in this work, should produce comparable charge and velocity conditions for secondary electron emission as in ref 68. The emitted electrons are accelerated with a high voltage of 25 kV toward a passivated implanted planar silicon (PIPS, Mirion Technologies) detector. The resulting spectra are fit with a Furry distribution, ^{69,70} which is a Polya distribution where b=1, to evaluate the electron yield.

Simulation input and output are available at the Materials Data Facility. 71,72

ASSOCIATED CONTENT

s Supporting Information

The Supporting Information is available free of charge at https://pubs.acs.org/doi/10.1021/acs.nanolett.4c00356.

Additional details of experiments and simulations, secondary electrons at different temperatures, and the numerical methods for calculating the kinetic energy spectrum (PDF)

AUTHOR INFORMATION

Corresponding Author

André Schleife — Department of Materials Science and Engineering, Materials Research Laboratory, and National Center for Supercomputing Applications, University of Illinois at Urbana—Champaign, Urbana, Illinois 61801, United States; orcid.org/0000-0003-0496-8214; Email: schleife@illinois.edu

Authors

Yifan Yao — Department of Materials Science and Engineering, University of Illinois at Urbana—Champaign, Urbana, Illinois 61801, United States; orcid.org/0009-0003-0331-3766

Alina Kononov — Center for Computing Research, Sandia National Laboratories, Albuquerque, New Mexico 87123, United States; orcid.org/0000-0002-6600-224X

Arne Metzlaff – University of Duisburg-Essen, Faculty of Physics and CENIDE, 47057 Duisburg, Germany

Andreas Wucher – University of Duisburg-Essen, Faculty of Physics and CENIDE, 47057 Duisburg, Germany

Lukas Kalkhoff – University of Duisburg-Essen, Faculty of Physics and CENIDE, 47057 Duisburg, Germany

Lars Breuer — University of Duisburg-Essen, Faculty of Physics and CENIDE, 47057 Duisburg, Germany; ocid.org/0000-0002-7797-9662

Marika Schleberger — University of Duisburg-Essen, Faculty of Physics and CENIDE, 47057 Duisburg, Germany; orcid.org/0000-0002-5785-1186

Complete contact information is available at: https://pubs.acs.org/10.1021/acs.nanolett.4c00356

Notes

The authors declare no competing financial interest.

ACKNOWLEDGMENTS

We thank Zhihao Jiang, Richard Arthur Wilhelm, and Anna Niggas for valuable scientific discussions. This material is based upon work supported by the National Science Foundation under Grant Nos. OAC-2209857 and OAC-1740219 and by the Deutsche Forschungsgemeinschaft (DFG, German Research Foundation) Project No. 278162697-SFB 1242. A.S. acknowledges support by the Mercator Fellow Program of SFB 1242. A.K. was partially supported by the US Department of Energy Science Campaign 1 and Sandia National Laboratories' Laboratory Directed Research and Development (LDRD) Project No. 233196. An award of computer time was provided by the Innovative and Novel Computational Impact on Theory and Experiment (INCITE) program. This research used resources of the Argonne Leadership Computing Facility, which is a DOE Office of Science User Facility supported under Contract DE-AC02-06CH11357. This work made use of the Illinois Campus Cluster, a computing resource that is operated by the Illinois Campus Cluster Program (ICCP) in conjunction with the National Center for Supercomputing Applications (NCSA) and which is supported by funds from the University of Illinois at Urbana-Champaign. This article has been coauthored by an employee of National Technology & Engineering Solutions of Sandia, LLC under Contract No. DE-NA0003525 with the U.S. Department of Energy (DOE). The authors own all right, title and interest in and to the article and are solely responsible for its contents. The United States Government retains and the publisher, by accepting the article for publication, acknowledges that the United States Government retains a nonexclusive, paid-up, irrevocable, worldwide license to publish or reproduce the published form of this article or allow others to do so, for United States Government purposes. The DOE will provide public access to these results of federally sponsored research in accordance with the DOE Public Access Plan https://www.energy.gov/downloads/doepublic-access-plan.

REFERENCES

- (1) Fox, D.; Zhou, Y. B.; O'Neill, A.; Kumar, S.; Wang, J. J.; Coleman, J. N.; Duesberg, G. S.; Donegan, J. F.; Zhang, H. Z. Helium ion microscopy of graphene: Beam damage, image quality and edge contrast. *Nanotechnology* **2013**, *24*, 335702.
- (2) Iberi, V.; Vlassiouk, I.; Zhang, X.-G.; Matola, B.; Linn, A.; Joy, D. C.; Rondinone, A. J. Maskless Lithography and in situ Visualization of Conductivity of Graphene using Helium Ion Microscopy. *Sci. Rep.* **2015**, *5*, 11952.
- (3) Hlawacek, G.; Veligura, V.; van Gastel, R.; Poelsema, B. Helium ion microscopy. J. Vac. Sci. Technol., B: Nanotechnol. Microelectron.: Mater., Process., Meas., Phenom. 2014, 32, 020801.
- (4) Werner, W. S. M.; Astašauskas, V.; Ziegler, P.; Bellissimo, A.; Stefani, G.; Linhart, L.; Libisch, F. Secondary Electron Emission by Plasmon-Induced Symmetry Breaking in Highly Oriented Pyrolytic Graphite. *Phys. Rev. Lett.* **2020**, *125*, 196603.
- (5) Niggas, A.; Schwestka, J.; Balzer, K.; Weichselbaum, D.; Schlünzen, N.; Heller, R.; Creutzburg, S.; Inani, H.; Tripathi, M.; Speckmann, C.; McEvoy, N.; Susi, T.; Kotakoski, J.; Gan, Z.; George, A.; Turchanin, A.; Bonitz, M.; Aumayr, F.; Wilhelm, R. A. Ion-Induced Surface Charge Dynamics in Freestanding Monolayers of Graphene and MoS₂ Probed by the Emission of Electrons. *Phys. Rev. Lett.* 2022, 129, 086802.
- (6) Wellershoff, S.-S.; Hohlfeld, J.; Güdde, J.; Matthias, E. The role of electron—phonon coupling in femtosecond laser damage of metals. *Appl. Phys. A: Mater. Sci. Process.* **1999**, *69*, S99.

- (7) Chung, M. S.; Everhart, T. E. Simple calculation of energy distribution of low-energy secondary electrons emitted from metals under electron bombardment. *J. Appl. Phys.* **1974**, *45*, 707.
- (8) Petrov, Y.; Vyvenko, O. Secondary electron emission spectra and energy selective imaging in helium ion microscope. In *Proc. SPIE* 8036, Scanning Microscopies 2011: Advanced Microscopy Technologies for Defense, Homeland Security, Forensic, Life, Environmental, and Industrial Sciences; Newbury, D. E., Platek, S. F., Joy, D. C.; Maugel, T. K., Eds.; Orlando, FL, 2011; p 80360O.
- (9) Ullah, R.; Artacho, E.; Correa, A. A. Core Electrons in the Electronic Stopping of Heavy Ions. *Phys. Rev. Lett.* **2018**, *121*, 116401.
- (10) Ullah, R.; Corsetti, F.; Sánchez-Portal, D.; Artacho, E. Electronic stopping power in a narrow band gap semiconductor from first principles. *Phys. Rev. B* **2015**, *91*, 125203.
- (11) Shukri, A. A.; Bruneval, F.; Reining, L. *Ab Initio* electronic stopping power of protons in bulk materials. *Phys. Rev. B* **2016**, *93*, 035128.
- (12) Lee, C.-W.; Schleife, A. Hot-Electron-Mediated Ion Diffusion in Semiconductors for Ion-Beam Nanostructuring. *Nano Lett.* **2019**, 19, 3939.
- (13) Correa, A. A. Calculating electronic stopping power in materials from first principles. *Comput. Mater. Sci.* **2018**, *150*, 291.
- (14) Schleife, A.; Kanai, Y.; Correa, A. A. Accurate atomistic first-principles calculations of electronic stopping. *Phys. Rev. B* **2015**, *91*, 014306.
- (15) Lee, C.-W.; Stewart, J. A.; Dingreville, R.; Foiles, S. M.; Schleife, A. Multiscale simulations of electron and ion dynamics in self-irradiated silicon. *Phys. Rev. B* **2020**, *102*, 024107.
- (16) Bernardi, M.; Vigil-Fowler, D.; Lischner, J.; Neaton, J. B.; Louie, S. G. *Ab Initio* Study of Hot Carriers in the First Picosecond after Sunlight Absorption in Silicon. *Phys. Rev. Lett.* **2014**, *112*, 257402.
- (17) Brown, A. M.; Sundararaman, R.; Narang, P.; Goddard, W. A.; Atwater, H. A. Nonradiative Plasmon Decay and Hot Carrier Dynamics: Effects of Phonons, Surfaces, and Geometry. *ACS Nano* **2016**, *10*, 957.
- (18) Brown, A. M.; Sundararaman, R.; Narang, P.; Schwartzberg, A. M.; Goddard, W. A.; Atwater, H. A. Experimental and *Ab Initio* Ultrafast Carrier Dynamics in Plasmonic Nanoparticles. *Phys. Rev. Lett.* **2017**, *118*, 087401.
- (19) Kononov, A.; Schleife, A. Pre-equilibrium stopping and charge capture in proton-irradiated aluminum sheets. *Phys. Rev. B* **2020**, *102*, 165401.
- (20) Kononov, A.; Schleife, A. Anomalous Stopping and Charge Transfer in Proton-Irradiated Graphene. *Nano Lett.* **2021**, *21*, 4816.
- (21) Vázquez, H.; Kononov, A.; Kyritsakis, A.; Medvedev, N.; Schleife, A.; Djurabekova, F. Electron cascades and secondary electron emission in graphene under energetic ion irradiation. *Phys. Rev. B* **2021**, *103*, 224306.
- (22) Geelen, D.; Jobst, J.; Krasovskii, E. E.; van der Molen, S. J.; Tromp, R. M. Nonuniversal Transverse Electron Mean Free Path through Few-layer Graphene. *Phys. Rev. Lett.* **2019**, *123*, 086802.
- (23) Kononov, A.; Olmstead, A.; Baczewski, A. D.; Schleife, A. First-principles simulation of light-ion microscopy of graphene. *2D Materials* **2022**, *9*, 045023.
- (24) Elzinga, P. A.; Lytle, F. E.; Jian, Y.; King, G. B.; Laurendeau, N. M. Pump/probe spectroscopy by asynchronous optical sampling. *Appl. Spectrosc.* **1987**, *41*, 2.
- (25) Sokolowski-Tinten, K.; von der Linde, D. Ultrafast phase transitions and lattice dynamics probed using laser-produced x-ray pulses. *J. Phys.: Condens. Matter* **2004**, *16*, R1517.
- (26) López-Martens, R.; Varjú, K.; Johnsson, P.; Mauritsson, J.; Mairesse, Y.; Salières, P.; Gaarde, M. B.; Schafer, K. J.; Persson, A.; Svanberg, S.; Wahlström, C.-G.; L'Huillier, A. Amplitude and Phase Control of Attosecond Light Pulses. *Phys. Rev. Lett.* **2005**, *94*, 033001.
- (27) Hentschel, M.; Kienberger, R.; Spielmann, C.; Reider, G. A.; Milosevic, N.; Brabec, T.; Corkum, P.; Heinzmann, U.; Drescher, M.; Krausz, F. Attosecond metrology. *Nature* **2001**, *414*, 509.

- (28) Agostini, P.; DiMauro, L. F. The physics of attosecond light pulses. *Rep. Prog. Phys.* **2004**, *67*, 813.
- (29) Kirchmann, P. S.; Bovensiepen, U. Ultrafast electron dynamics in Pb/Si(111) investigated by two-photon photoemission. *Phys. Rev. B* **2008**, *78*, 035437.
- (30) Sandhofer, M.; Sklyadneva, I.Yu.; Sharma, V.; Trontl, V. M.; Zhou, P.; Ligges, M.; Heid, R.; Bohnen, K.-P.; Chulkov, E.; Bovensiepen, U. Unoccupied electronic structure and relaxation dynamics of Pb/Si(1 1 1). *J. Electron Spectrosc. Relat. Phenom.* **2014**, 195, 278.
- (31) Thiemann, F.; Sciaini, G.; Kassen, A.; Lott, T. S.; Horn-von Hoegen, M. Disentangling the electronic and lattice contributions to the dielectric response of photoexcited bismuth. *Phys. Rev. B* **2024**, *109*, L041105.
- (32) Kalkhoff, L.; Matschy, S.; Meyer, A. S.; Lasnig, L.; Junker, N.; Mittendorff, M.; Breuer, L.; Schleberger, M. Ultra-large polymer-free suspended graphene films. *arXiv*, November 14, 2023, 2311.08137, ver. 1. DOI: 10.48550/arXiv.2311.08137
- (33) Breuers, A.; Herder, M.; Kucharczyk, P.; Schleberger, M.; Sokolowski-Tinten, K.; Wucher, A. A concept to generate ultrashort ion pulses for pump-probe experiments in the keV energy range. *New J. Phys.* **2019**, *21*, 053017.
- (34) Kucharczyk, P.; Golombek, A.; Wucher, A. Generation of ultrashort ion pulses in the keV range: Numerical simulations. *Nuclear Instruments and Methods in Physics Research Section B: Beam Interactions with Materials and Atoms* **2020**, 483, 41.
- (35) Golombek, A.; Breuer, L.; Danzig, L.; Kucharczyk, P.; Schleberger, M.; Sokolowski-Tinten, K.; Wucher, A. Generation of ultrashort keV Ar⁺ ion pulses via femtosecond laser photoionization. *New J. Phys.* **2021**, 23, 033023.
- (36) Kalkhoff, L.; Golombek, A.; Schleberger, M.; Sokolowski-Tinten, K.; Wucher, A.; Breuer, L. Path to ion-based pump-probe experiments: Generation of 18 ps keV Ne⁺ ion pulses from a cooled supersonic gas beam. *PRRESEARCH* **2023**, *5*, 033106.
- (37) Mihaila, M. C. C.; Szabo, G. L.; Redl, A.; Goldberger, M.; Niggas, A.; Wilhelm, R. A. Generation of Picosecond Ion Pulses by Ultrafast Electron-Stimulated Desorption. *arXiv*, October 4, 2023, 2310.02631, ver. 1. DOI: 10.48550/arXiv.2310.02631.
- (38) Gruber, E.; Wilhelm, R. A.; Pétuya, R.; Smejkal, V.; Kozubek, R.; Hierzenberger, A.; Bayer, B. C.; Aldazabal, I.; Kazansky, A. K.; Libisch, F.; Krasheninnikov, A. V.; Schleberger, M.; Facsko, S.; Borisov, A. G.; Arnau, A.; Aumayr, F. Ultrafast electronic response of graphene to a strong and localized electric field. *Nat. Commun.* **2016**, 7, 13948.
- (39) Ueda, Y.; Suzuki, Y.; Watanabe, K. Quantum dynamics of secondary electron emission from nanographene. *Phys. Rev. B* **2016**, 94, 035403.
- (40) Ueda, Y.; Suzuki, Y.; Watanabe, K. Secondary-electron emission from multi-layer graphene: Time-dependent first-principles study. *Applied Physics Express* **2018**, *11*, 105101.
- (41) Tsubonoya, K.; Hu, C.; Watanabe, K. Time-dependent density-functional theory simulation of electron wave-packet scattering with nanoflakes. *Phys. Rev. B* **2014**, *90*, 035416.
- (42) Ritzau, S. M.; Baragiola, R. A. Electron emission from carbon foils induced by keV ions. *Phys. Rev. B* **1998**, *58*, 2529.
- (43) Kishinevsky, L. M. Estimation of electron potential emission yield dependence on metal and ion parameters. *Radiation Effects* **1973**, *19*, 23.
- (44) Baragiola, R. A.; Alonso, E. V.; Florio, A. O. Electron emission from clean metal surfaces induced by low-energy light ions. *Phys. Rev. B* **1979**, *19*, 121.
- (45) Schwestka, J.; Niggas, A.; Creutzburg, S.; Kozubek, R.; Heller, R.; Schleberger, M.; Wilhelm, R. A.; Aumayr, F. Charge-Exchange-Driven Low-Energy Electron Splash Induced by Heavy Ion Impact on Condensed Matter. *J. Phys. Chem. Lett.* **2019**, *10*, 4805.
- (46) Yu, Y.-J.; Zhao, Y.; Ryu, S.; Brus, L. E.; Kim, K. S.; Kim, P. Tuning the Graphene Work Function by Electric Field Effect. *Nano Lett.* **2009**, *9*, 3430.

- (47) Yan, R.; Zhang, Q.; Li, W.; Calizo, I.; Shen, T.; Richter, C. A.; Hight-Walker, A. R.; Liang, X.; Seabaugh, A.; Jena, D.; Grace Xing, H.; Gundlach, D. J.; Nguyen, N. V. Determination of graphene work function and graphene-insulator-semiconductor band alignment by internal photoemission spectroscopy. *Appl. Phys. Lett.* **2012**, *101*, 022105.
- (48) Lakits, G.; Aumayr, F.; Heim, M.; Winter, H. Threshold of ion-induced kinetic electron emission from a clean metal surface. *Phys. Rev. A* **1990**, *42*, 5780.
- (49) Zhao, S.; Kang, W.; Xue, J.; Zhang, X.; Zhang, P. Comparison of electronic energy loss in graphene and bn sheet by means of time-dependent density functional theory. *J. Phys.: Condens. Matter* **2015**, 27, 025401.
- (50) Weitzel, K.-M.; Mähnert, J.; Penno, M. ZEKE-PEPICO investigations of dissociation energies in ionic reactions. *Chem. Phys. Lett.* **1994**, 224, 371.
- (51) Zhou, Y.; Fox, D. S.; Maguire, P.; O'Connell, R.; Masters, R.; Rodenburg, C.; Wu, H.; Dapor, M.; Chen, Y.; Zhang, H. Quantitative secondary electron imaging for work function extraction at atomic level and layer identification of graphene. *Sci. Rep.* **2016**, *6*, 21045.
- (52) Duvenbeck, A.; Sroubek, F.; Sroubek, Z.; Wucher, A. Computer simulation of low-energy electronic excitations in atomic collision cascades. *Nuclear Instruments and Methods in Physics Research Section B: Beam Interactions with Materials and Atoms* **2004**, 225, 464.
- (53) Zarkadoula, E.; Daraszewicz, S. L.; Duffy, D. M.; Seaton, M. A.; Todorov, I. T.; Nordlund, K.; Dove, M. T.; Trachenko, K. Electronic effects in high-energy radiation damage in iron. *J. Phys.: Condens. Matter* **2014**, *26*, 085401.
- (54) Tsai, H.-L.; Jiang, L. Fundamentals of energy cascade during ultrashort laser-material interactions (Invited Paper). In *Proceedings Volume 5713, Photon Processing in Microelectronics and Photonics IV*; Fieret, J., Herman, P. R., Okada, T., Arnold, C. B., Bachmann, F. G., Hoving, W., Washio, K., Lu, Y., Geohegan, D. B., Trager, F., Dubowski, J. J., Eds.; San Jose, CA, 2005; p 343.
- (55) Castro, A.; Marques, M. A. L.; Rubio, A. Propagators for the time-dependent Kohn-Sham equations. *J. Chem. Phys.* **2004**, *121*, 3425.
- (56) Gómez Pueyo, A.; Marques, M. A. L.; Rubio, A.; Castro, A. Propagators for the Time-Dependent Kohn-Sham Equations: Multistep, Runge-Kutta, Exponential Runge-Kutta, and Commutator Free Magnus Methods. J. Chem. Theory Comput. 2018, 14, 3040.
- (57) Zangwill, A.; Soven, P. Resonant Photoemission in Barium and Cerium. *Phys. Rev. Lett.* **1980**, *45*, 204.
- (58) Zangwill, A.; Soven, P. Resonant two-electron excitation in copper. *Phys. Rev. B* **1981**, *24*, 4121.
- (59) Vanderbilt, D. Optimally smooth norm-conserving pseudopotentials. *Phys. Rev. B* **1985**, 32, 8412.
- (60) Kononov, A.; Lee, C.-W.; Dos Santos, T. P.; Robinson, B.; Yao, Y.; Yao, Y.; Andrade, X.; Baczewski, A. D.; Constantinescu, E.; Correa, A. A.; Kanai, Y.; Modine, N.; Schleife, A. Electron dynamics in extended systems within real-time time-dependent density-functional theory. MRS Commun. 2022, 12, 1002.
- (61) Draeger, E.; Gygi, F. *Qball*; Github, Inc., 2017. https://github.com/LLNL/qball (accessed 04-03-2024).
- (62) Schleife, A.; Draeger, E. W.; Anisimov, V. M.; Correa, A. A.; Kanai, Y. Quantum Dynamics Simulation of Electrons in Materials on High-Performance Computers. *Computing in Science & Engineering* **2014**, *16*, 54.
- (63) Draeger, E. W.; Andrade, X.; Gunnels, J. A.; Bhatele, A.; Schleife, A.; Correa, A. A. Massively parallel first-principles simulation of electron dynamics in materials. *Journal of Parallel and Distributed Computing* **2017**, *106*, 205.
- (64) Mermin, N. D. Thermal Properties of the Inhomogeneous Electron Gas. *Phys. Rev.* **1965**, *137*, A1441.
- (65) Åberg, D.; Erhart, P.; Lordi, V. Contributions of point defects, chemical disorder, and thermal vibrations to electronic properties of $Cd_{1-x}Zn_x$ Te alloys. *Phys. Rev. B* **2013**, *88*, 045201.

- (66) Aumayr, F.; Lakits, G.; Winter, H. On the measurement of statistics for particle-induced electron emission from a clean metal surface. *Appl. Surf. Sci.* **1991**, *47*, 139.
- (67) Schrempf, D.; Meissl, W.; Aumayr, F. An ultra-compact setup for measuring ion-induced electron emission statistics. *Nuclear Instruments and Methods in Physics Research Section B: Beam Interactions with Materials and Atoms* **2013**, 317, 44.
- (68) Wittkower, A. B.; Betz, H. D. Equilibrium-charge-state distributions of energetic ions (z > 2) in gaseous and solid media. *Atomic Data and Nuclear Data Tables* 1973, 5, 113.
- (69) Furry, W. H. On Fluctuation Phenomena in the Passage of High Energy Electrons through Lead. Phys. Rev. 1937, 52, 569.
- (70) Dietz, L. A.; Sheffield, J. C. Secondary electron emission induced by 5–30-keV monatomic ions striking thin oxide films. *J. Appl. Phys.* **1975**, *46*, 4361.
- (71) Blaiszik, B.; Chard, K.; Pruyne, J.; Ananthakrishnan, R.; Tuecke, S.; Foster, I. The Materials Data Facility: Data Services to Advance Materials Science Research. *JOM* **2016**, *68*, 2045.
- (72) Yao, Y.; Kononov, A.; Metzlaff, A.; Wucher, A.; Kalkhoff, L.; Breuer, L.; Schleberger, M.; Schleife, A. Non-equilibrium dynamics of electron emission from cold and hot graphene under proton irradiation. *The Materials Data Facility*, 2024. DOI: 10.18126/1cpb-sj41.